Investigation on the Acoustic Behavior of a Turbulent Swirl-Stabilized Combustor Fed with Liquid Fuel

Ayane Johchi[1, *], Laurent Zimmer[2, 3], Mamoru Tanahashi[1]

1: Department of Mechanical and Aerospace Engineering, Tokyo Institute of Technology,
2-12-1 Ookayama, Meguro-ku, Tokyo 152-8550, Japan
2: CNRS, UPR 288, Laboratoire d'Énergétique Moléculaire et Macroscopique, Combustion (EM2C),
Grande Voie des Vignes, 92290 Châtenay-Malabry, France
3: Ecole Centrale Paris, Grande Voie des Vignes, 92290 Châtenay-Malabry, France
* correspondent author: ajohchi@navier.mes.titech.ac.jp

Abstract

Burners operating in lean premixed prevaporized (LPP) regimes are considered as a good candidate to reduce the pollutant emissions from gas turbines. Lean combustion regimes provide a uniform lean mixture of fuel and air that burns at lower temperature than non-premixed flames, mainly reducing thermal NOx emissions. However, combustion in this regime often faces stability issues. In particular, the coupling of heat release and pressure oscillations in the combustor can produce self-excited oscillations. In addition, the flame that is stabilized by swirling flow motion in gas turbine combustor is strongly affected by energetic large-scale coherent flow structure known as Precessing Vortex Core (PVC). In the present work a swirl-stabilized combustor fed with liquid fuel (dodecane) is used for the investigation of combustion instability, structure of PVC and their relative strength. The droplet and velocity field distributions are characterized using High Speed Particle Imaging Velocimetry. The acoustic pressure fluctuations are measured close to the injection device and on the combustion chamber axis. CH* chemiluminescence is also measured as an indicator of the reaction rate in the flame. The frequency and amplitude of the acoustic and aero-dynamical instability are investigated varying the global equivalence ratio. In order to give detailed insight into the flow dynamics, dynamic mode decomposition (DMD) is introduced. Performing Multi-variable DMD on Mie scattering intensity signal, velocity distribution and acoustic pressure signal, the two dominant structures are captured at each frequency associated to acoustic instability and PVC. Using amplitude spectrum of DMD, its relative strength can be calculated. It is revealed that the strength of PVC tends to be high in the low equivalence ratio conditions while it seems to drop in ϕ > 0.55 conditions. Instead of that, the strength of the acoustics mode shows constant increase with the equivalence ratio. It likely indicates that the strong fluctuating cycle associated to acoustic mode may interfere with the coherent structure of PVC in high equivalence ratio cases. The correlation coefficients of reconstructed DMD mode at PVC frequency in each condition show high value at low equivalence ratio conditions and the values decrease with equivalence ratio increase. It explains that the acoustic pressure oscillation interferes with the coherent structure of PVC and its effect becomes stronger with equivalence ratio increase.

1. Introduction

Due to environmental concerns, permissible pollutant emissions of gas turbine plant or aircraft engines have been significantly decreased in recent years (Correa, 1998). Combustion in gas turbines was traditionally based on nonpremixed flames for various reasons (safety, stability), but this type of combustion leads to large pollutant emissions (NOx, CO, ...). To face this issue, lean premixed prevaporized (LPP) regimes are envisaged in new generation combustors (Moore, 1997; Lefebvre, 1995; Tacina, 1990). This concept consists in providing a uniform lean mixture of fuel and air that burns at lower temperature than nonpremixed flames, mainly reducing thermal NOx emissions. Unfortunately gas turbines operating in lean conditions often present high combustion dynamics, leading to stability issues such as combustion instabilities, flashback, self-ignition, and blowout (Lieuwen et al, 2005). In particular, the coupling of heat release and pressure oscillations in the combustor can produce self-excited oscillations of such an amplitude that they may damage the combustor (Lefebvre, 1999; Nauert et al, 2007; Candel, 2002). It is known that these thermo-acoustic instabilities tend to develop more easily in partially and perfectly premixed combustion systems such as the LPP ones (Ducruix et al. 2003).

In gas turbine combustor, the flames are aero-dynamically stabilized by swirling flow. In addition to the

thermo-acoustic instability, the swirl-stabilized flame is strongly affected by energetic large-scale coherent flow structure. Recently large-scale helical vortex structures that precess around the combustor (Precessing Vortex Core: PVC) gain a great interest, which is often observed in swirl-stabilized combustor (Froud et al, 1995; Syred, 2006; Wegner et al, 2004). The occurrence and strength of PVC depends on swirl number (Gupta, 1984; Syred and Beer, 1974), the mode of fuel entry and equivalence ratio. For gaseous premixed or non-premixed fuels, both acoustic and aerodynamic instability have been widely investigated (Boxx et al, 2010; Meier et al, 2010; Stöhr et al, 2011). However, liquid fueled combustion has unique processes such as atomization and evaporation. These processes make the mechanism more complicated and difficult to investigate.

In the present work a swirl-stabilized combustor fed with liquid fuel (dodecane) is used for the investigation of combustion instability. Using similar configuration, which is called as liquid-fuel lean direct fuel injection (LDI) combustion, combustion instability has been recently investigated (Yi and Santavicca, 2012; De la Cruz Garcia et al, 2009). In this study, frequency and amplitude of the acoustic and aero-dynamical instability are investigated varying the global equivalence ratio. In order to give detailed insight into the flow dynamics, dynamic mode decomposition (DMD) is introduced.

2. Experimental Setup

2.1 Gas turbine model combustor

The gas turbine model combustor used in this study was originally developed as a multi-injection burner and the different stabilization processes were investigated (Providakis et al, 2012, 2013). In the present study, only the primary (pilot) stage is used to generate a swirl-stabilized flame. The injection device is composed of two stages where air and liquid fuel can flow and mix. The resulting mixture enters a rectangular combustion chamber (500 x 150 x 150 mm^3), composed of two silica windows for optical access and two water-cooled walls. The water flow rate is regulated so that the water exit temperature remains constant for all operating conditions. The injector is composed of a pressurized nozzle for fuel distribution and a swirler for air injection. The pressurized nozzle generates a solid cone and fuel can be injected at a maximum flow rate of 6.3 $l{\cdot}h^{-1}$. Its flow number is equal to 1.4 $l{\cdot}h^{-1}{\cdot}bar^{-0.5}$. The air swirler is composed of 18 vanes and it is geometrically designed so that 13 % of the global air rate flows through this stage. Swirler is designed so that the swirl number S based on geometrical considerations is close to 1 (Galley et al, 2011). To enhance fuel vaporization, air is preheated at 473 K.

2.2 Spray Characterization and Velocity Measurements

The spray is characterized using High Speed Particle Image Velocimetry (HSPIV) in the axial direction. It was decided to use fuel droplets as particle tracers (no seeding). The camera collects the Mie scattering signal from individual droplets traversing the laser sheet. The laser sheet is generated by a system consisting

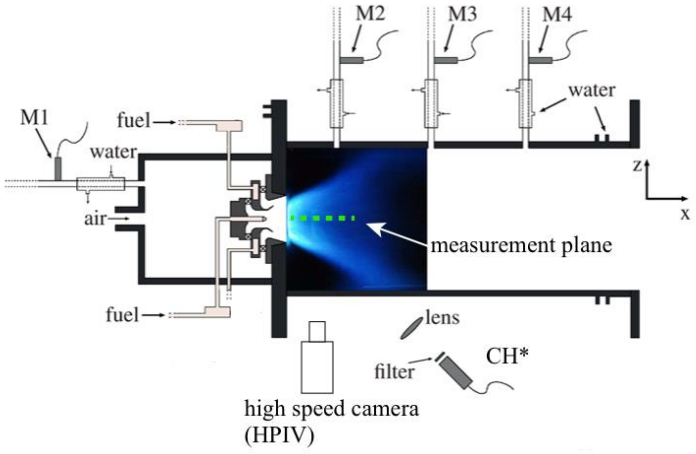

Fig. 1 Schematic view of the experimental setup (flow from left to right)

of two Nd:YAG lasers (Quantronix). Both lasers emit pulses at a wavelength of 532 nm with an energy of 5 mJ per pulse and a temporal width of 120 ns and at a frequency of 10 kHz. An optical system (Melles Griot) is used to convert the laser beam into a planar light sheet 100 mm wide and 1 mm thick. Both sides of the combustion chamber include large rectangular silica windows. For the axial measurements, two small rectangular quartz windows (100 mm long and 15 mm wide) were designed and placed in the upper and lower walls of the combustion chamber, allowing the laser sheet to cross the chamber in the axial direction on its centerline. A fast speed camera (Photron Fastcam SA5, 1024 x 1024 pixels at 6000 frames per second) equipped with a 105 mm F /2.8 Nikon Nikkor objective is used to acquire the resulting images. The two lasers work at half the camera's acquisition frequency (f_{cam} = 20 kHz) and are synchronized by a pulse delay generator (BNC 555 pulse/delay Generator). The time delay, Δt, between two pulses has been set to 20 μs so that the displacement of a droplet does not exceed one fourth of the processing window size, which is 48 x 48 pixels in this study. Measurement regions are set to 90 x 150 mm and the camera resolution is determined to be 776 x 448 pixels, which means that the spatial resolution of PIV is about 9 mm for 48 x 48 pixels interrogation region. Note that the velocity vectors are evaluated with 67 % overlap. In this sense, velocity vectors are obtained every 6 mm. In this study, a high spatial resolution PIV algorithm (Tanahashi et al, 2002, 2008) is used to calculate the two-dimensional velocity field from successive particle images obtained by the high-speed camera. The elimination scheme is mainly used for cut off of the high wave number noise that exceeds the spatial resolution of PIV. The high wave number noise is introduced by overlap of the interrogation regions.

2.3 Pressure and Heat Release Fluctuations

Three Bruel and Kjaer microphones (M1, M3 and M4) are placed in semi-infinite water cooled waveguides. Microphone M1 is flush mounted in plenum while M3 and M4 are placed in the middle and downstream of combustion chamber to measure pressure fluctuations. A photomultiplier (Hamamatsu, H5784-04), coupled with a filter (λ = 408 ± 10 nm) and a spherical lens (focal = 300 mm) to collect all the light emitted by the flame, is used to measure global CH* chemiluminescence, which is an indicator of the reaction rate in the flame. All signals are acquired simultaneously on a multi-port acquisition card (National Instruments), at a rate of 16 kHz during 1.6 seconds for the HSPIV measurements. Details of the measurement system can be found in (Providakis et al, 2013).

3. Operating Conditions

Table 1 shows the operating conditions chosen for the present study. To investigate the effect of equivalence ratio on the instability, the measurements are conducted by changing equivalence ratio in the ϕ = 0.4 to 0.7 range. There are two ways to change equivalence ratio: decreasing air or increasing fuel. Therefore, there are two series of data set. For the first one, the amount of fuel is kept constant while the equivalence ratio is varied from 0.4 to 0.7 (PC_{40} - PC_{70}), keeping the power produced by the burner constant. The other is that the global air flow rate are constant (FC_{40} - FC_{70}) and the amount of fuel is varied with the constant global air flow field. Note that PC_{50} and FC_{50} are both same air flow condition and fuel injection. As a reference, measurements are also conducted with non-reactive cases with both same air flow and same fuel injection as PCs and FCs.

Table 1 Operating conditions

ϕ		$\dot{m}_a$ [$g \cdot s^{-1}$]	$\dot{m}_f$ [$g \cdot s^{-1}$]	P_w [kW]		$\dot{m}_a$ [$g \cdot s^{-1}$]	$\dot{m}_f$ [$g \cdot s^{-1}$]	P_w [kW]
0.40	PC_{40}	40.4	1.02	45.2	FC_{40}	32.3	0.819	36.2
0.45	PC_{45}	35.9	1.02	45.2	FC_{45}	32.3	0.921	40.7
0.50	PC_{50}	32.3	1.02	45.2	FC_{50}	32.3	1.02	45.2
0.55	PC_{55}	29.4	1.02	45.2	FC_{55}	32.3	1.13	49.7
0.60	PC_{60}	26.9	1.02	45.2	FC_{60}	32.3	1.23	54.2
0.65	PC_{65}	24.9	1.02	45.2	FC_{65}	32.3	1.33	58.7
0.70	PC_{70}	23.1	1.02	45.2	FC_{70}	32.3	1.43	63.2

4. Results and Discussions

4.1 Flames and Droplets Structure

The mean droplet velocity magnitude and reacting field in the three operating conditions (PC_{50}, PC_{55} and PC_{70}) are shown in fig.2. Contour line of the velocity magnitude is superimposed on the natural emission images. The mean fields are computed using 5,000 images for each operating condition. The droplet velocity is only computed in the region where the droplet's Mie intensity signal, which is acquired during the HSPIV campaign, shows averagely significant value. For all condition within this measurement, the flame presents a V-shape structure.

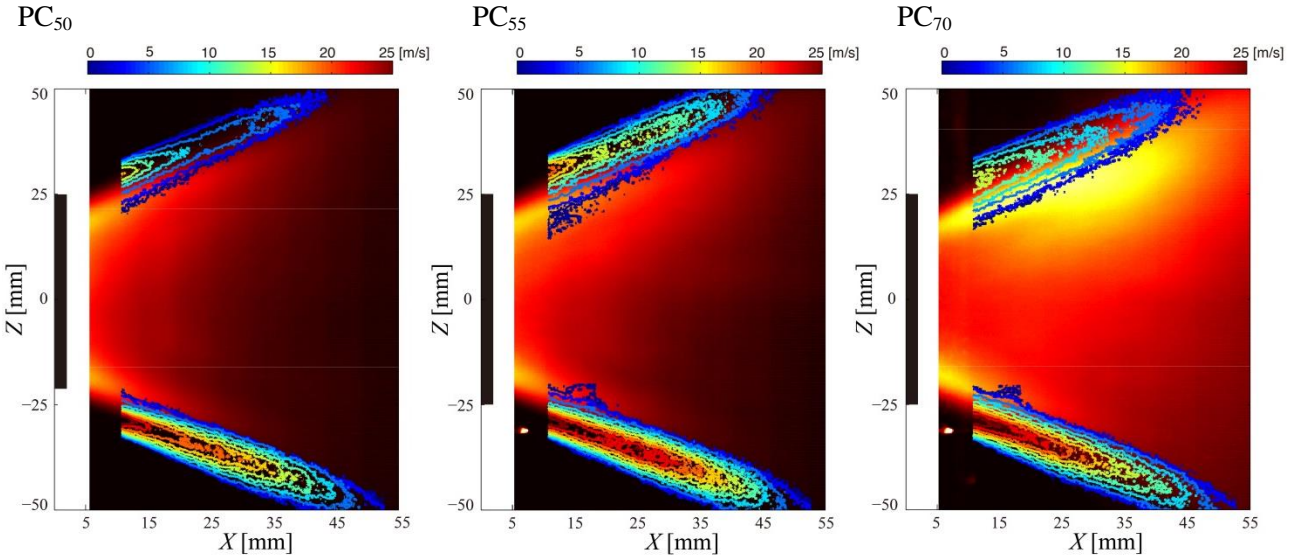

Fig. 2 Average droplet velocity magnitude and natural emission intensity field for the three operating conditions (PC_{50}, PC_{55} and PC_{70}). Contour line of the velocity magnitude is superimposed on the natural emission image. Note that the natural emission image is not Adel transform image but integral value.

4.2 Acoustic Measurements and HSPIV

To characterize the dynamic behavior, a spectral analysis is performed on the acoustic pressure and CH* spontaneous emission and velocity fluctuation near the nozzle exit. Figure 3 shows power spectrum density (PSD) of velocity magnitude near the nozzle exit (X = 12 mm, Z = -27 mm) for two operating conditions, PC_{70} (ϕ = 0.70) and PC_{40} (ϕ = 0.40) with fixing the power produced by the burner at 45.2 kW. The PSD is computed using the Welch method. In the higher equivalence ratio condition (PC_{70}, Fig. 3(left)), the velocity fluctuation show strong peak centered at f_{ac} = 308 Hz as expected by the Rayleigh criterion in the case of thermo-acoustic instabilities. Similar frequency is also seen in the acoustic pressure fluctuation as well as CH* chemiluminescence (Figures are not shown here). With decreasing equivalence ratio, the amplitude of the peak at acoustic is getting weaker. In the lowest equivalent ratio condition (PC_{40}) shown in Fig. 3 (right), the peak corresponding to thermo-acoustic instability is no longer observed. Instead, one can see a strong peak centered at $f_{PVC} \approx$ 2044 Hz, which represents aerodynamic instability corresponding to the helical structure known as the precessing vortex core (PVC). As it is known that the frequency of the PVC is a function of the flow rate, the higher equivalence ratio condition shows lower frequency due to its lower flow rate to keep the power constant. Note that the relatively weak peak is still observed in acoustic pressure fluctuation and CH* chemiluminescence. The spectra show same tendency in the case with constant air flow rate (FC_{40} - FC_{70}). The interaction between acoustic and PVC can be also seen in the spectrum of CH* chemiluminescence at low equivalence ratio conditions (FC_{40}-FC_{50} and PC_{40}-PC_{50}) as a peak with very low amplitude at frequency of the sum and difference of the acoustic and PVC ones ($f_{PVC} \pm f_{ac}$).

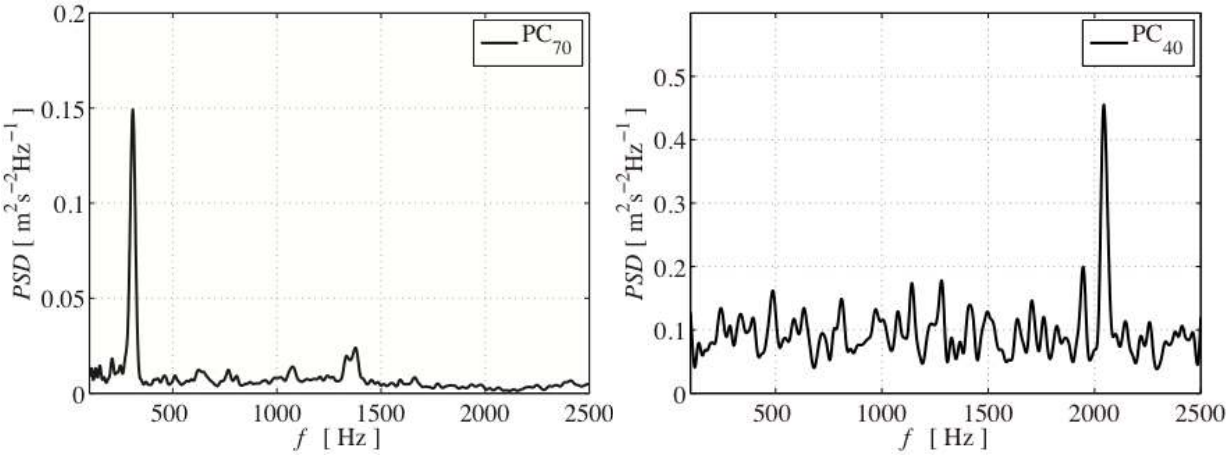

Fig. 3 Power Spectrum Density (PSD) of the velocity fluctuation near the swirler nozzle for $\phi = 0.70$ (left) and for $\phi = 0.40$ (right) with constant power.

4.3 Dynamic Mode Decomposition (DMD) analyses

To characterize the dynamics of the flow field, Dynamic Mode Decomposition (DMD) is used in this study. DMD is introduced by Schmid (2010, 2011) as a mathematical tool capable to extract dynamic information from numerical or experimental data. The extracted information is referred as a generalization of global stability modes that can be used to characterize the dynamics of a system. The DMD algorithm is applied to the Mie scattering intensity and velocity field, respectively. The amplitude spectrum of the DMD on the Mie scattering detected distinct peak at frequency associated to PVC. However, the peak at frequency associated to acoustic instability cannot be seen in the spectrum at low equivalence ratio conditions, which is seen in the PSD of acoustic pressure fluctuation. To detect coherent structure in different variables, one uses the multi-variable DMD algorithm (Richecoeur et al, 2012). The multi-variable DMD is applied to the reactive turbulent flows and its capability is shown by Richecoeur et al (2012). In present study, 500 samples are used on the velocity field, Mie scattering and simultaneously measured acoustic pressure at the middle of combustion chamber (M3).

4.3.1 Amplitude spectrum of the DMD

In Fig. 4, the amplitude spectra of the DMD for two operating conditions are displayed. Left spectrum is for PC_{70} and right one is for PC_{40}. In this analysis, the local frequency resolution around the frequency of interest (the PVC frequency) is about 20 Hz, which is half of the resolution that is expected in PSD with same length dataset. In the higher equivalence ratio condition, the spectra reveals high amplitude and relatively wide peak at 288 and 320 Hz which coincide with the one observed from PSD of local velocity magnitude f_{ac} = 308 Hz. It also shows low amplitude peak centered at f_{PVC} = 1381 Hz. As expected from the PSD of local velocity

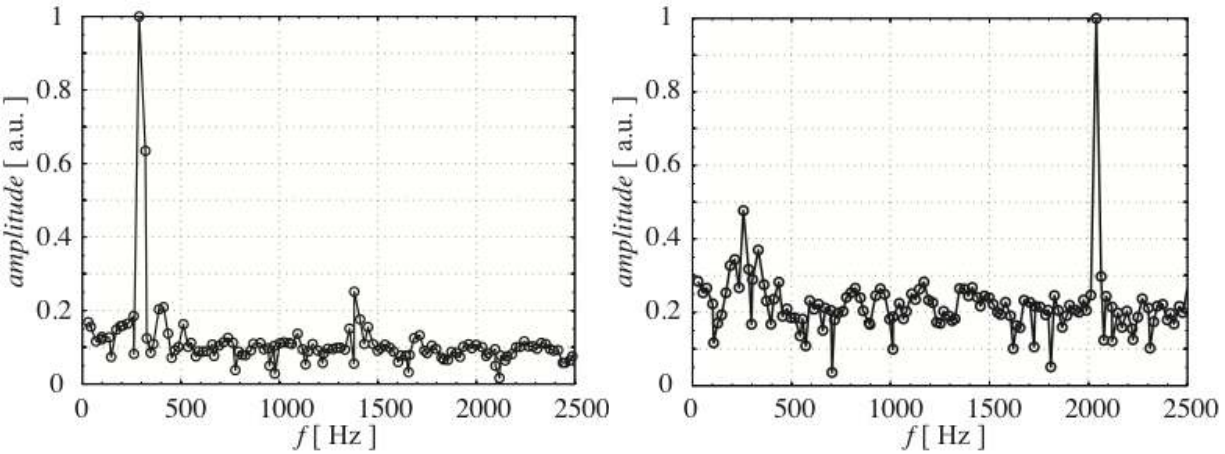

Fig. 4 Amplitude spectrum of the multi-variable DMD for two operating conditions: PC_{70} (left) and PC_{40} (right)

magnitude, the amplitude of the acoustic peak decreases relative to aerodynamic peak with decreasing equivalence ratio. The spectrum in the lowest equivalence ratio case (PC_{40}) shows narrower strong peak centered at f_{PVC} = 2040 which coincides with that in PSD of the local velocity fluctuation.
As discussed by Richecoeur et al, (2012), the DMD result is strongly affected by the last snapshot. To minimize the effect on the result, the 1.5 seconds measurement data is divided into 30 successive and separate blocks that have 500 snapshots each. Then the multi-variable DMD technique is applied to these blocks as if they were different data sets but for the same flow condition. Figure 5 shows the frequency associated to PVC detected in spectrum in each cases. The black circles and crosses represent the frequency for the each data set of FCs (circle) and PCs (cross). The red square (FCs) and blue triangle (PCs) filled markers show the mean value with standard deviation as error bars. The PVC frequencies of PCs case show almost linear decrease with equivalence ratio increase while that of FCs slightly increase from 1680 Hz to 1800 Hz. The higher equivalence ratio in FCs condition means that the higher power is put in some air flow condition. The change in the series of data sets of FCs might be caused by the change of temperature in the chamber and consequent sound velocity change. The standard deviation tends to be bigger in the higher equivalence ratio cases. One reason of the higher dispersion of the data in high equivalence ratio cases is that the peak of the spectra at the PVC frequency is much lower than in lower equivalence ratio case.

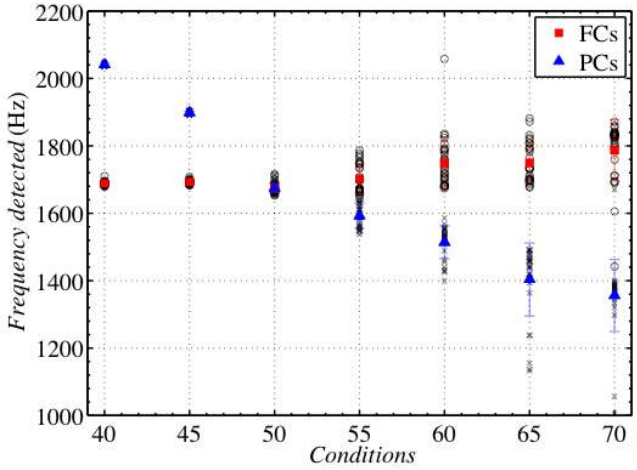

Fig. 5 Detected PVC frequency from multi-variable DMD for each condition.

To analyze the strength of PVC from the spectrum, one must be careful because the multi-variable DMD contains Mie signal which depends on the droplet size. It changes when equivalence ratio is different. To allow comparisons between the runs, an "intensity" of the impact of the PVC on the flame is computed from the DMD spectrum as the height of the peak at the PVC frequency divided by the baseline (mean value between f_{PVC} - 200 Hz and f_{PVC} + 200 Hz). Figure 6 show the PVC intensity in the both cases of FCs (left) and PCs (right). The circles show the values in each data set and filled markers are the mean value with standard deviation as an error bar. The variability of this treatment is around ± 0.5, which is quite high but the amount of runs enable tendencies to be drawn. For both cases, the strength tends to be high in the low equivalence ratio conditions ($FC_{40,\ 45}$ and $PC_{40,\ 45}$) while it seems to drop in $\phi > 0.55$. The PVC strength seems to depend on equivalence ratio and one cannot see clear difference in its tendency between two sets of data: changing equivalence ratio with air flow rate constant (FCs) or power constant (PCs).
The strength of the acoustic modes is also calculated in the same manner as for PVC mode. Figure 7 show the relative intensity of acoustic mode in the both cases of FCs (left) and PCs (right). The strength of the acoustics fluctuation shows constant increase with the equivalence ratio. Note that the relative strength of the acoustic mode in PCs is growing more rapidly with equivalence ratio than that of FCs because the flow rate decreases with equivalence ratio to keep the power constant. As a result the acoustic mode becomes more dominant in high equivalence ratio condition.
These two figures Fig.6 and 7 show that the helical structures is strongly detected in the low equivalence ratio conditions and decreases with the equivalence ratio. Instead of that, the strong fluctuating cycle that is associated to the acoustic mode of the chamber is dominant in these higher conditions. An assumption one can make here is the strong acoustic mode may interfere with the PVC structure in high equivalence ratio cases.

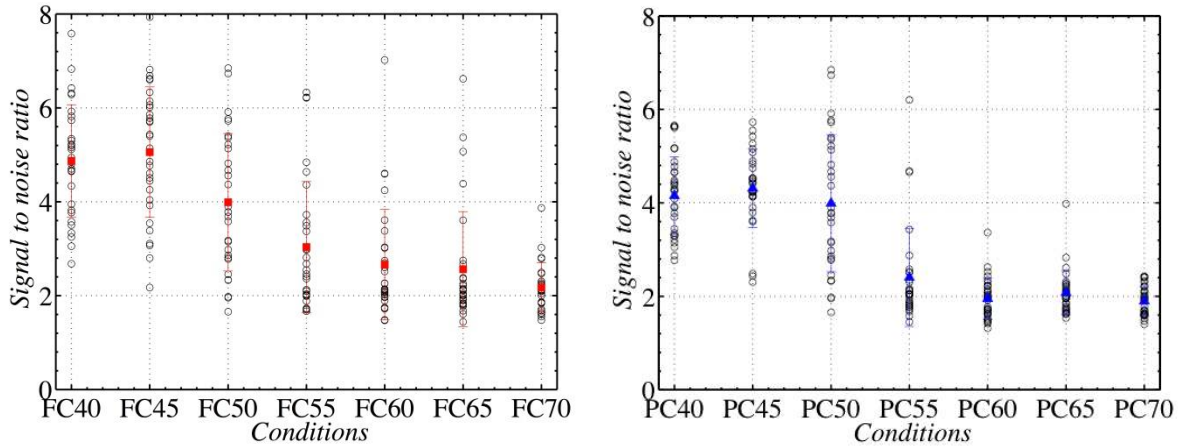

Fig. 6 The strength of PVC as a function of equivalence ratio with constant air flow rate (left) and constant power produced by the burner (right).

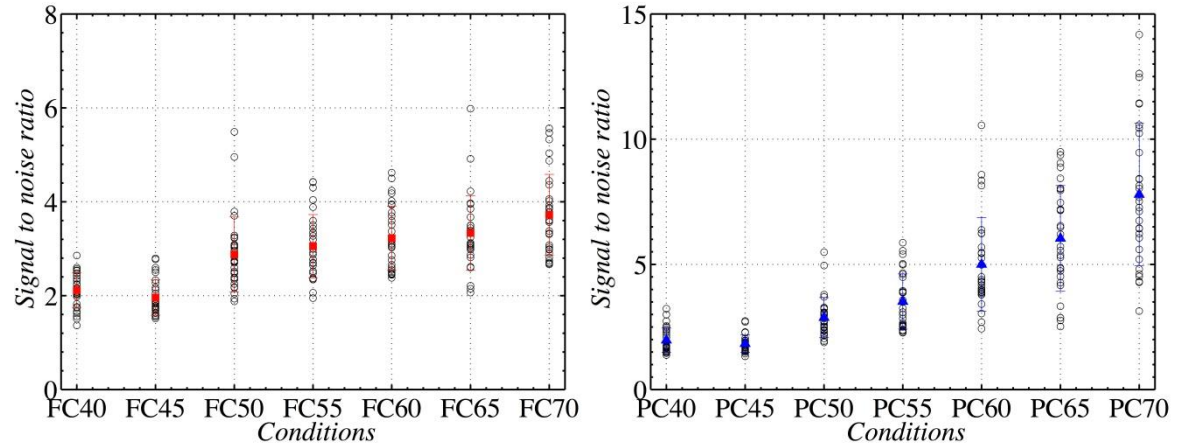

Fig. 7 The strength of acoustic mode as a function of equivalence ratio with constant air flow rate (left) and constant power produced by the burner (right).

4.3.2 Reconstruction of the fluctuating cycle of PVC and Acoustic Modes

The following analysis focuses on three operating conditions: ϕ = 0.50 case FC/PC_{50}, ϕ = 0.70 case with keeping air flow constant FC_{70} and keeping power constant PC_{70}. The purpose of this analysis is to observe the influence of the equivalence ratio changes on the PVC structure.

Figure 8 (a) (b) and (c) show reconstructed DMD mode associated to the frequency of PVC for the first phase and 90° for the three case (FC_{50} (a), FC_{70} (b) and PC_{70} (c)). Although velocity and acoustic pressure data are also used for the Multi-variable DMD analysis, the DMD mode is reconstructed only on Mie scattering data. The red circle in the amplitude spectrum shown in the left represents the frequency of reconstructed mode. Red regions represent positive value and blue region is negative. Contours of 25% Mie scattering intensity (black line) are added. Lower half of the mode is shown here. All conditions present an opposite behavior between the lower and upper region of the chamber, resulting from the asymmetric structure of the PVC. In the strong PVC condition (fig.8 (a)), the structure lines up alternatively in the direction of the jet injection. The spatial distribution of the PVC mode is very similar in all low equivalence ratio conditions ($FC_{40\text{-}50}$ and $PC_{40\text{-}50}$). On the other hand, each spatial cell (positive or negative) of the weak PVC condition (FC_{70} and PC_{70}, fig.8 (b) and (c)) extends in length towards downstream. Whole structure also stretches and penetrates into deeper region in the chamber. Figure 8 (d) shows reconstructed DMD mode associated to the frequency of acoustic mode. For this case, opposite half is symmetric. The global structure is much different from that of PVC modes. Instead of the alternative structure, each structure reaches deeper region and the fluctuating cycle shows oblique oscillation. The thermo-acoustic instability corresponds to the quarter-wave mode of the combustion chamber. As a result of the acoustic pressure, the droplet motion is shown in the fluctuating cycle of reconstructed mode associated to acoustic perturbation.

As discussed in above, the helical structure exhibits strong structure in the low equivalence ratio condition and its strength decrease with the equivalence ratio increase while the acoustic oscillation is becoming stronger. A concern here is if the spatial structure of PVC itself alters with equivalence ratio change or the helical structure is coherent in any condition and its strength just getting weaker. To determine the coherence of the spatial distribution of modes associated to the frequency of PVC in each mode, correlation coefficient of each run is calculated. Figure 9 shows the correlation coefficient of the reconstructed mode between FC_{50} and the other cases. The correlation coefficient is calculated up to 20 mm from the injection exit since oscillations of the flow due to the PVC are usually intense close to the nozzle (Stöhr et al. 2011; Moeck et al. 2012). Top two figures of Fig.9 show the correlation coefficient in air flow constant conditions (FCs). Figure 9 (a) is for the case of the reactive case and (b) is for the case of non-reactive sprays with both same air flow and same fuel injection condition as FCs as a reference case. The filled markers show the mean value with standard deviation as error bars. In the low equivalence ratio conditions, FC_{40} and FC_{45} in fig. 9 (a), the correlation coefficient is very high (>0.9) and its variation is small. It means that the structure of PVC is coherent in low equivalence ratio conditions as expected from fig. 8 (a). It is interesting to note that the correlation coefficient in FC_{50} distribute with bigger variance while the values itself are still high. With increasing equivalence ratio, the mean value decrease and its variation increase. In the non-reactive cases (fig.9 (b)), the mean correlation coefficient remain high (>0.8) in high equivalence ratio conditions. This means that the changes in the spray do not alter the PVC structure. The decrease of the value can be seen higher equivalence ratio case than FC_{50}. This correspond the change in PVC strength in fig. 6 (a). It may explain that the acoustic pressure oscillation interferes with the coherent structure of PVC and the effect becomes stronger with equivalence ratio increase. Figure 9 (c) and (d) are for the condition of power constant (PCs) with reactive (c) and non-reactive (d). The same tendency can be seen with power constant conditions although the value itself is lower than that with air flow rate constant conditions. The correlation coefficient between different cases is relatively low even in the condition of non-reactive flow since global flow field is different each other and PVC is the function of air flow rate. The fact that coherence in the reactive case is higher than that of non-reactive case is due to heat release tends to stabilize the flow inside the injector. One may therefore conclude that when there is no interaction between PVC and acoustic mode, the spatial structure is relatively stable.

Summary and Conclusion

In this study, a swirl-stabilized combustor fed with liquid fuel (dodecane) is used for the investigation of combustion instability, structure of PVC and their relative strength. The droplet and velocity field distributions are characterized using High Speed Particle Imaging Velocimetry. The acoustic pressure fluctuations are also measured close to the injection device and on the combustion chamber axis. CH* chemiluminescence is also measured as an indicator of the reaction rate in the flame. The frequency and amplitude of the acoustic and aero-dynamical instability are investigated varying the global equivalence ratio. The PSDs of the velocity fluctuation, acoustic pressure and CH* show strong peak in phase as expected by the Rayleigh criterion in the case of thermo-acoustic instabilities. With decreasing equivalence ratio, the amplitude of the peak at acoustic is getting weak. In the lowest equivalent ratio condition, the peak correspond to thermo-acoustic instability is no longer observed. Instead, one can see strong peak at frequency associated to aerodynamic instability corresponds to the helical structure known as the precessing vortex core (PVC). In order to give detailed insight into the flow dynamics, dynamic mode decomposition (DMD) is introduced. Performing Multi-variable DMD on Mie intensity signal, velocity distribution and acoustic pressure signal, the two dominant structures are captured at each frequency associated to acoustic instability and PVC. Using amplitude spectrum of DMD, its relative strength can be calculated. It is revealed that the strength of PVC tends to be high in the low equivalence ratio conditions while it seems to drop in ϕ > 0.55 conditions. Instead of that, the strength of the acoustics mode shows constant increase with the equivalence ratio. It likely indicates that the strong fluctuating cycle associated to acoustic mode may interfere with the coherent structure of PVC in high equivalence ratio cases. The correlation coefficients of reconstructed DMD mode at PVC frequency in each condition show high value at low equivalence ratio conditions and the values decrease with equivalence ratio increase. It explains that the acoustic pressure oscillation interferes with the coherent structure of PVC and its effect becomes stronger with equivalence ratio increase.

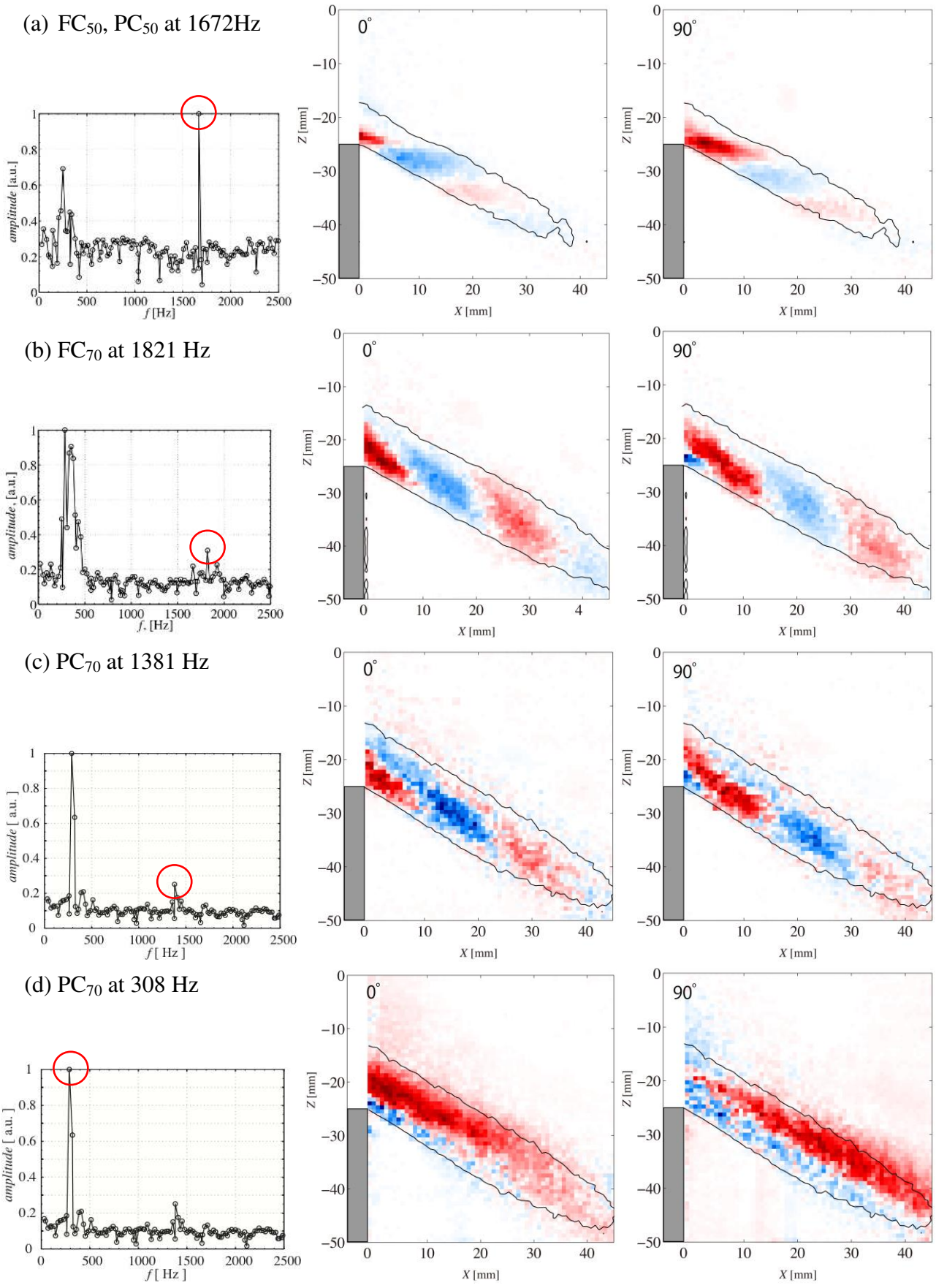

Fig. 8 Reconstructed DMD mode associate with PVC frequency for the operating condition (a) PC/FC$_{50}$, (b) FC$_{70}$ (c) PC$_{70}$, and acoustic mode for the condition (d) PC$_{70}$. Contours of 25% Mie scattering intensity (black line) are added.

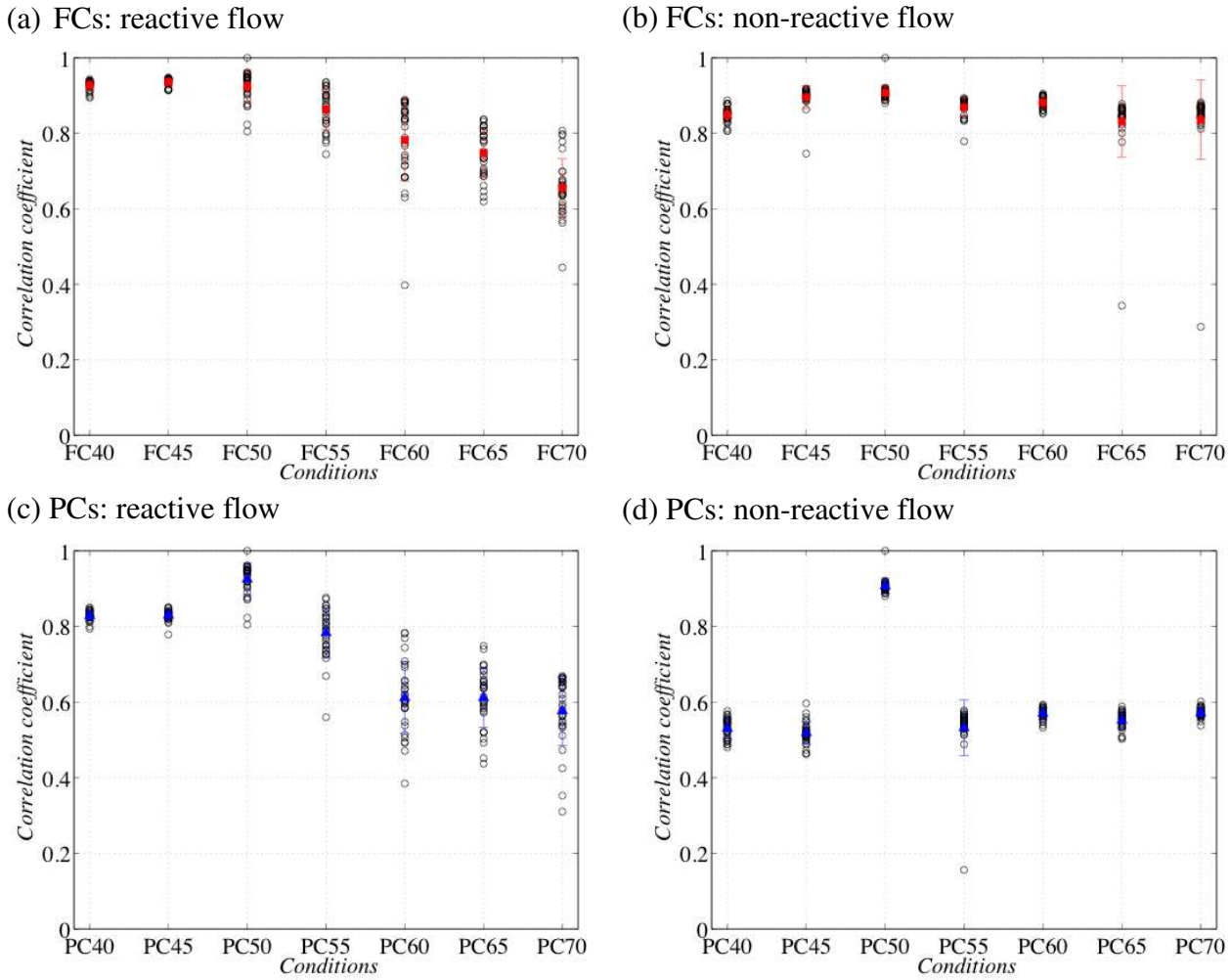

Fig. 9 The correlation coefficient of DMD mode associated to PVC frequency between equivalent ratio 0.50 case (FC50, PC50) and others. Reactive (left) and Non-Reactive (right) case. Constant air flow rate (Top) and constant power produced by the burner (bottom)

Acknowledgments

The first author would like to thank the European Commission and the Erasmus Mundus framework for their mobility fellowship offered by the EM-BEAM program coordinated by Ecole Centrale Paris.

References

Boxx I, Stöhr M, Carter C, MeierW (2010) Temporally resolved planar measurements of transient phenomena in a partially pre-mixed swirl flame in a gas turbine model combustor. Combustion and Flame 157(8):1510–1525

Candel S (2002) Combustion dynamics and control: progress and challenges. Proceedings of the combustion institute 29(1):1–28

Correa SM (1998) Power generation and aeropropulsion gas turbines: from combustion science to combustion technology. In: Symposium (International) on Combustion, Elsevier, vol 27, pp 1793–1807

De la Cruz Garcia M, Mastorakos E, Dowling A (2009) Investigations on the self-excited oscillations in a kerosene spray flame. Combustion and Flame 156(2):374–384

Ducruix S, Schuller T, Durox D, Candel S (2003) Combustion dynamics and instabilities: Elementary coupling and driving mechanisms. Journal of Propulsion and Power 19(5):722–734

Froud D, O'doherty T, Syred N (1995) Phase averaging of the precessing vortex core in a swirl burner under piloted and premixed combustion conditions. Combustion and Flame 100(3):407–412

Galley D, Ducruix S, Lacas F, Veynante D (2011) Mixing and stabilization study of a partially premixed swirling flame using laser induced fluorescence. Combustion and Flame 158(1):155–171

Gupta AK (1984) Swirl flows. Technomic Publishing Co., Lancaster, PA

Lefebvre A (1995) The role of fuel preparation in low-emission combustion. Journal of engineering for gas turbines and power 117(4):617–654

Lefebvre AH (1999) Gas turbine combustion. Taylor & Francis

Lieuwen TC, Yang V, Lu FK (2005) Combustion instabilities in gas turbine engines: operational experience, fundamental mechanisms and modeling. American Institute of Aeronautics and Astronautics

Meier W, Boxx I, St¨ohr M, Carter C (2010) Laser-based investigations in gas turbine model combustors. Experiments in fluids 49(4):865–882

Moeck, J. P., J.-F. Bourgouin, D. Durox, T. Schuller, and S. Candel (2012). Nonlinear interaction between a precessing vortex core and acoustic oscillations in a turbulent swirling flame. Combustion and Flame 159 (8):2650–2668.

Moore M (1997) Nox emission control in gas turbines for combined cycle gas turbine plant. Proceedings of the Institution of Mechanical Engineers, Part A: Journal of Power and Energy 211(1):43–52

Nauert A, Petersson P, Linne M, Dreizler A (2007) Experimental analysis of flashback in lean premixed swirling flames: conditions close to flashback. Experiments in fluids 43(1):89–100

Providakis T, Zimmer L, Scouflaire P, Ducruix S, et al (2012) Characterization of the acoustic interactions in a two-staged multi-injection combustor fed with liquid fuel. Journal of Engineering for Gas Turbines and Power 134(11)

Providakis T, Zimmer L, Scouflaire P, Ducruix S (2013) Characterization of the coherent structures in swirling flames stabilized in a two-staged multi-injection burner: Influence of the staging factor. Comptes Rendus Mecanique 341(1):4–14

Richecoeur F, Hakim L, Renaud A, Zimmer L, et al (2012) Dmd algorithms for experimental data processing in combustion. Proceeding of the 2012 Summer Program pp 459–468

Schmid PJ (2010) Dynamic mode decomposition of numerical and experimental data. Journal of Fluid Mechanics 656(1):5–28

Schmid PJ (2011) Application of the dynamic mode decomposition to experimental data. Experiments in fluids 50(4):1123–1130

Stöhr M, Boxx I, Carter C, Meier W (2011) Dynamics of lean blowout of a swirl-stabilized flame in a gas turbine model combustor. Proceedings of the Combustion Institute 33(2):2953–2960

Syred N (2006) A review of oscillation mechanisms and the role of the precessing vortex core (pvc) in swirl combustion systems. Progress in Energy and Combustion Science 32(2):93–161

Syred N, Beer J (1974) Combustion in swirling flows: a review. Combustion and Flame 23(2):143–201

Tacina, R. (1990). Low NOx potential of gas turbine engines. AIAA Aerospace Sciences Meeting and Exhibit, 28th, (90-0550):3

Tanahashi M, Ootsu M, Fukushima M, Miyauchi T (2002) Measurement of coherent fine scale eddies in turbulent mixing layer by dpiv. Engineering Turbulence Modelling and Experiments 5, Elsevier Science 525–534

Tanahashi M, Hirayama T, Taka S, Miyauchi T (2008) Measurement of fine scale structure in turbulence by time-resolved dual-plane stereoscopic piv. International Journal of Heat and Fluid Flow 29(3):792–802

Wegner B, Maltsev A, Schneider C, Sadiki A, Dreizler A, Janicka J (2004) Assessment of unsteady rans in predicting swirl flow instability based on les and experiments. International journal of heat and fluid flow 25(3):528–536

Yi T, Santavicca D (2012) Combustion instability and flame structure of turbulent swirl-stabilized liquid-fueled combustion. Journal of Propulsion and Power 28(5):1000–1014